Structure, Stability and (non) Reactivity of the Low-Index Surfaces of Crystalline B_2O_3-I

Niveen W. Assaf,[1] Marco De La Pierre,[2] Mohammednoor K. Altarawneh,[1]* Marian W. Radny,[3,4†] Zhong-Tao Jiang,[1] Bogdan Z. Dlugogorski[1]

[1]School of Engineering and Information Technology

Murdoch University, 90 South Street, Murdoch, WA 6150, Australia

[2]Curtin Institute for Computation, Department of Chemistry, Curtin University, P.O. Box U1987, Perth, WA 6845, Australia

[3]School of Mathematical and Physical Sciences, The University of Newcastle

Callaghan, NSW 2308, Australia

[4]Institute of Physics, Poznan University of Technology, Poznan, Poland

[†] *Corresponding Authors:

* Phone: (+61) 8 9360-7507

E-mail: M.Altarawneh@Murdoch.edu.au

[†] Phone: (+61) 2 4921-5447

E-mail: Marian.Radny@Newcastle.edu.au

Abstract

Diboron trioxide (B_2O_3) assumes critical importance as an effective oxidation inhibitor in prominent chemical applications. For instance, it has been extensively used in electrolysis and ceramic/glass technology. Results are presented of accurate quantum mechanical calculations using the PW1PW hybrid HF/DFT functional of four low-index surfaces of the low-pressure phase of B_2O_3: (101), (100), (011) and (001). Bond lengths, bond angles and net Mulliken charges of the surface atoms are analysed in detail. Total and projected density of states as well as surface energies are discussed. Occurrence of tetrahedral BO_4 units on the lowest energy structures of two of these surfaces has been demonstrated for the first time. The corresponding surface orientations incur larger energies in reference to the two orientations featuring only BO_3 units. All of the four investigated lowest energy structures have no dangling bonds, which reasonably relates to the experimentally observed low reactivity of this compound. Findings in this paper pave the way for potential interest in perspective of future studies on the surfaces of amorphous B_2O_3, as well as on the hydroxylation of both crystalline and amorphous B_2O_3.

1. Introduction

Diboron trioxide (B_2O_3) is one of the most widely deployed oxidation inhibitors[1, 2] and as such finds direct applications in electrolysis,[3] ceramic and glass technology.[4-6] At ambient conditions, B_2O_3 adopts a vitreous (amorphous) form, v-B_2O_3. Earlier studies[7-9] on v-B_2O_3 reported its structure as composed of randomly oriented BO_3 building blocks, in which three oxygen atoms located at the corners of a triangle surround a boron atom. However, an experimental study by Jellison et al.[10] involving the ^{17}O isotope revealed that oxygen in v-B_2O_3 occupies two distinct sites, depending on whether an oxygen atom forms part of a boroxol ring or whether it links two boroxol rings. Each boroxol ring represents a hexagon with three alternating vertices occupied by B atoms and the other three by O atoms. In addition, each B coordinates to an additional O, which in turn bonds to a B atom on an adjacent ring. Thus, a boroxol ring (B_3O_6) comprises three BO_3 triangles, with one oxygen atom in each triangle lying on the outer of the ring. Subsequent experimental investigations have yielded similar conclusions.[11-13]

Over a wide range of operational pressures and temperatures, crystalline B_2O_3 exhibits two crystallographic structures - B_2O_3-I at low pressure[14] and B_2O_3-II at high pressure.[15, 16] At a pressure of 400 MPa (> 483.15 K), the amorphous form of B_2O_3 transforms into crystalline B_2O_3-I. The planar triangles of BO_3 present in B_2O_3-I form a hexagonal structure (space group $P3_121$) with lattice parameters of a = 4.33 Å and c = 8.34 Å.[14, 17] With increasing pressure, the optimal coordination number of boron atoms changes from a three-fold to a four-fold arrangement.[18, 19] At ~6.5 GPa (> 1000 K),[16, 18, 20] the second B_2O_3–II crystal structure is formed, which consists of three-dimensional networks of tetrahedral units of BO_4 adopting an orthorhombic lattice (space group $Ccm2_1$). Two in three oxygens in this structure form dative bonds and have a three-fold rather than two-fold coordination, resulting in the

BO_4 tetrahedra being disorted, with 3 B-O lengths larger than the 4th one (1.51 vs 1.37 Å).[15] Note that the three-fold coordinated boron in B_2O_3-I has got a sp^2 hybridisation, with an empty low-energy p orbital in the valence shell that is mainly responsible for the Lewis acid behaviour of this compound. In the case of the high pressure phase B_2O_3–II, acceptance of an electron pair into this orbital results in a sp^3 hybridization and the observed distorted four-fold coordination.[21]

Despite the amorphous form being the most exploited in practical applications, the crystalline phases can serve as significant model systems to get insights into the properties of B_2O_3, especially at an atomistic scale. As regards the structure and energetics of B_2O_3-I surfaces, Bredow and Islam[22] are so far the only authors in the literature to have investigated them by means of quantum mechanical methods. In their pioneering work, they focused on the low-index surfaces and found the following stability order: (101) < $(1\bar{1}1)$ (or, equivalently, (011)) < (100) < (001). Notably, the authors found out that 3 out of the 4 investigated surfaces feature dangling bonds, which partially contrasts with the experimental observation of B_2O_3 surfaces not being reactive.

In this paper, we report the results from a comprehensive investigation on the low-index (*hkl*) surfaces of B_2O_3-I, as obtained through hybrid Hartree-Fock/Density Functional Theory (HF/DFT) calculations. Building on the early work by Bredow and Islam,[22] we have explored sp^3 in addition to sp^2 hybridised surface boron, as well as alternative atomic arrangements for surface terminations, and have successfully identified new lowest energy surface structures, providing significant connections with the inertness of B_2O_3 and the structure of its vitreous form.

2. Computational methodology

Calculations were performed using the ab initio CRYSTAL14 code.[23, 24] Surfaces were simulated by using the 2D periodic slab model, consisting of a film formed by a set of atomic layers parallel to the *hkl* crystalline plane of interest. All the calculations were performed at the DFT level. In particular, the PW1PW Hamiltonian was adopted,[25] which contains a hybrid HF/DFT exchange term, that has already been used in previous studies on B_2O_3.[22, 26] Additional calculations were performed using the PW91,[27] PBEsol[28] (GGA), B3LYP[29-31] and PBE0[32] (hybrid) Hamiltonians. Hybrid functionals have been successfully applied to the investigation of surfaces of a variety of minerals, including diamond,[33] silica,[34, 35] spinel[36] and olivine.[37, 38]

In CRYSTAL, the multi-electronic wave-function is constructed as an anti-symmetrized product (Slater determinant) of mono-electronic crystalline orbitals (COs) which are linear combinations of local functions (i.e. atomic orbitals, AOs) centred on each atom of the crystalline structure. In turn, AOs are linear combinations of Gaussian-type functions (GTF, the product of a Gaussian times a real solid spherical harmonic to give *s*-, *p*- and *d*-type AOs). In the present study, boron and oxygen were described by the m-6-311G(d) basis-sets proposed by Heyd et al. to investigate a large set of semiconductor solids.[39] The exponents (in units of $bohr^{-2}$) of the most diffuse sp shells are 0.16 (B) and 0.26 (O), whereas the exponents of the d shells are 0.80 (B) and 1.29 (O).

DFT Exchange and correlation contributions were numerically evaluated by integrating, over the cell volume, functions of the electron density and of its gradient. Choice of the integration grid is based on an atomic partition method, originally developed by Becke.[40] In the present study, the extra-large pruned (75, 974) *p* grid was chosen (XLGRID in the code[24]), which

ensures a satisfactory accuracy in the integrated electron charge density, the corresponding error for the studied surfaces being smaller than $1 \cdot 10^{-4}$ |e| over either 408 [(101), (011) and (001)] or 476 [(100)] |e|. Diagonalization of the Hamiltonian for the studied surfaces was performed at either 13 [(101), (011) and (001)] or 16 [(100)] irreducible k points in the reciprocal space (Monkhrost net[41]) by setting the shrinking factor to 6 (more details are provided in ref. 24). The thresholds controlling the accuracy in the evaluation of Coulomb and exchange integrals (ITOL1, ITOL2, ITOL3, ITOL4 and ITOL5 in the code[24]) were set to 10^{-8} (ITOL1 to ITOL4) and 10^{-18} (ITOL5). Threshold on the SCF energy was set to 10^{-8} hartree. Structures were optimized by using the analytical energy gradients with respect to atomic coordinates[42-44] and a BFGS algorithm; convergence was checked on both gradient components and nuclear displacements, whose tolerances where set to 0.0003 Hartree·bohr^{-1} and 0.0012 bohr, respectively. Vibrational frequencies at the Γ point were computed within the harmonic approximation by numerical differentiation of the analytical gradients with respect to the atomic Cartesian coordinates[45]. This permitted to verify that the optimised structures lie on minima of the potential energy surface.

The specific surface energy γ at $T = 0$ K was calculated by using the following relation:[46]

$$\gamma = \lim_{n\to\infty} E_s(n) = \lim_{n\to\infty} \frac{E(n) - nE_{bulk}}{2A} \quad (1)$$

where $E(n)$ denotes the energy of a n-layer slab; E_{bulk} signifies the energy of the bulk; A is the area of the primitive unit cell of the surface; the factor 2 in the denominator accounts for the upper and lower surfaces of the slab. $E_s(n)$ is thus the energy per unit area required for the formation of the surface from the bulk. As more layers are added in the calculation ($n \rightarrow \infty$), $E_s(n)$ will converge to the surface energy per unit area (γ). All values were corrected for Basis Set Superposition Error (BSSE, e.g. ref. 46).

139 The number of atomic layers to be considered in each slab, *n*, was set to 60, and chosen to
140 satisfy the following criteria: surface energy for all orientations converged within 0.01 J/m^2,
141 bond lengths converged within 0.01 Å, bond angles converged within 1°.

142 2.1. Effect of the Hamiltonian

143 The impact of the choice of the Hamiltonian was analysed for both bulk and slab calculations,
144 by comparing the results obtained using PBEsol, PW91 (GGA), B3LYP, PBE0 and PW1PW
145 (hybrid). Table 1 shows cell parameters and B-O distances in bulk B_2O_3-I for the different
146 functionals. The most affected quantity turns out to be the *c* lattice parameter: whereas PBE0
147 and PW1PW reproduce it very well, yielding a +0.3 and +0.4% discrepancy compared to the
148 experiment, respectively, the other functionals show significant deviations: -2.9% (PBEsol),
149 +1.9% (PW91), +4.5% (B3LYP). The case of B3LYP is peculiar: even if this functional is
150 known to overestimate lattice parameters,[47] such a large overestimation probably relates to its
151 poorer description of dispersion interactions,[48] and suggests to avoid its use for the purposes
152 of the present investigation. On the other hand, both PBE0 and PW1PW show a nearly
153 coincident, excellent agreement with the experimental data, in line with the known accuracy
154 of hybrid methods; we decided to adopt PW1PW as the main method for the sake of
155 increased comparability with the previous work by Bredow and Islam.[22] As regards the *a* cell
156 parameter, B-O distances and O-B-O angles, all of them are always reproduced with an
157 accuracy better than 1%.

158

159 Let us now assess the adopted Hamiltonians against the surface energies of the four low-
160 index surfaces considered in this study (see Table 2). The most important aspect is that the
161 stability order is preserved regardless the adopted functional; the same applies for the overall
162 atomic arrangements of the surfaces (not reported). This outcome is very significant as it
163 implies that results presented in the following sections may be considered to be independent

from the chosen Hamiltonian. One minor point to note is that, in the case of the functionals with large *c* parameter discrepancies in the bulk, PW91 and B3LYP, the two lowest energy surfaces become more stabilised as opposed to the highest energy ones, as compared to the other functionals; on the contrary PBEsol (which largely underestimates *c* in the bulk) yields a relative destabilisation of the two lowest energy surfaces. The (100) surface orientation, i.e. the 2nd most stable, has the *c* parameter parallel to its plane and exhibits the largest dependence of its formation energy upon the *c* value.

3. Results and discussion

3.1. Bulk properties

The atomic structure of the hexagonal unit cell of B_2O_3-I, as obtained through our PW1PW simulations, is shown in Figure 1; it contains 6 B and 9 O atoms, 1 and 2 of which are irreducible by symmetry.[17, 49] The structure is made up of a three-dimensional network of planar BO_3 triangles,[14, 17] with three-fold coordinated, sp^2 hybridised B atoms.

Table 1 provides a set of structural and electronic properties, in excellent agreement with experimental measurements and theoretical data available in the literature:[17, 18, 26, 49-51] lattice parameters, bond lengths and angles, band gap, Mulliken net charges. Bond angles reveal a very limited distortion of the BO_3 groups from an ideal triangular coordination, as their values range between 116° and 123°. The full set of atomic coordinates is available in the output files provided as Supplementary Information.

Figure 2 displays the calculated total density of states (DOS) of bulk B_2O_3-I, as well as its projections on the B and O atoms. There is a wide insulating gap of 8.66 eV, which is consistent with the value reported by Bredow and Islam[22] (9.1 eV). The valence band

consists of two continuum regions of energy levels, the lower one stretching between -21.4 and -18.7 eV, and the upper one extending from -9.3 eV up to the top of the valence band. Except for the lower half of the latter, where there is a significant contribution from the B atomic orbitals, the valence band is mostly contributed by O orbitals. On the other hand, the bottommost portion of the conduction band (from +8.6 eV on) mainly relates to electronic states involving B orbitals.

3.2. Structure of the low-index surfaces

We started our analysis by considering all the plane orientations featuring 0, 1 or -1 in their Miller indices. Symmetry relations reduce this set to just six irreducible orientations: (100), (001), (011), (101), (110) and (111); in this regard, the $(1\bar{1}1)$ orientation presented by Bredow and Islam[22] is equivalent to (011) by symmetry. It was then noted that there exist no (110) nor (111) slabs with symmetry related surfaces, and then null perpendicular dipole moment. As a result, we ended up investigating four low-index surfaces: (001), (011), (100) and (101). Atomic structures of the lowest energy terminations for these surfaces are represented in Figure 3-6 (the corresponding coordinates are available in the output files provided as Supplementary Information); bond lengths and angles for the surface B atoms are listed in Table 3. At variance with the study by Bredow and Islam,[22] none of the atoms in these structures have got dangling bonds.

In the case of (101) and (100) orientations all surface borons are three-fold coordinated, with a nearly ideal triangular geometry that closely resembles the bulk case: bond lengths are in the range 1.339÷1.381 Å for (101) and 1.344÷1.371 Å for (100). These values compare well with 1.361÷1.371 Å in the bulk, the maximum shortening and lengthening being only 0.022

and 0.010 Å, respectively. Similarly, bond angles are 116.5÷124.1˚ in (101) and 116.2÷124.5˚ in (100), to be compared with 116.5÷122.8˚ in the bulk.

Interestingly, the other two orientations, (011) and (001), both feature four-fold coordinated B atoms and three-fold coordinated O atoms, which result in pronounced distortions from the bulk geometry. In the case of (011) one surface B atom out of five is four-fold coordinated (B4* in Figure 4 and Table 3), and one surface O atom out of six is three-fold coordinated (O7*). The B4* atom shows much longer bonds compared to the bulk: 1.400, 1.428 and 1.467 Å when bound to two-fold coordinated oxygens, up to 1.642 Å when bound to O7*; the corresponding bond angles are within 103.1÷116.3˚, indicating a distorted tetrahedral geometry. The remaining surface borons show large, though less marked, deviations from the bulk when bound to two-fold coordinated O atoms, with bond lengths spreading over the range 1.328÷1.411 Å; however, this quantity can raise up to 1.469 and 1.526 Å for the B-O7* bonds. Besides, all the three-fold coordinated borons show bond angles that are in line with a slightly distorted triangular geometry, 113.6÷126.6˚.

Finally, the (001) orientation has one four-fold coordinated surface boron in two (B2* in Figure 3 and Table 3) and one three-fold coordinated surface oxygen in three (O3*). The B2* atom forms bonds with three-fold coordinated oxygens whose length is moderately longer than in the bulk, 1.378÷1.431 Å, whereas the bond with O3* is as long as 1.847 Å; bond angles (101.3÷114.1˚) again suggest a distorted tetrahedral geometry. The only three-fold coordinated surface boron, B1, has short bonds with two-fold coordinated oxygens, 1.334 and 1.335 Å, and a 1.455 Å long bond with O3*; all bond angles involving B1 lie in the range 117.2÷123.5, which are typical for a triangular geometry.

3.3. Electronic properties of the low-index surfaces

Table 4 presents the Mulliken net charges for the surface B atoms and all the O atoms that are chemically bound to the former (charges for all the atoms in each slab are available in the output files provided as Supplementary Information). In general, surface atoms are less charged than in the bulk: compare the ranges +0.802÷+1.019 |e| and -0.522÷-0.710 |e| for three-fold coordinated B and two-fold coordinated O, respectively, with the bulk values of +1.029 |e| and -0.676, -0.705 |e|. In the case of B atoms, charges smaller than +0.89 |e| are only found in the surfaces which do not contain four-fold coordinated borons. As regards higher coordinated atoms (i.e. four-fold B and three-fold O), they carry larger charges than the average: in this case B values are very close to the bulk ones, +0.992 |e| in (011) and +0.986 |e| in (001), whereas O values are even larger than in the bulk, -0.797 |e| in (011) and -0.804 |e| in (001).

Figure 7 shows the total and projected DOS curves for the four low-index surfaces, indicating an insulating character for all of them. The band gap amounts to 8.57, 7.97, 8.53 and 8.50 eV for the (001), (011), (100) and (101) orientations, respectively (Bredow and Islam[22] report 8.5 eV for the (011) surface). The gap reduction as compared to the bulk crystal (8.66 eV) relates in all cases to the occurrence of occupied electronic states that lie just above the top of the valence band (which again agrees with the corresponding analysis by Bredow and Islam[22]).

3.4. Surface energies

Surface energy values for the investigated low-index surfaces, as calculated through Eq. (1), are reported in Table 2. The stability order is as follows: (101) < (100) < (011) < (001), corresponding to energies of 0.254, 0.396, 0.735 and 0.882 J/m^2, respectively. Interestingly,

263 the two orientations featuring only three-fold coordinated B atoms are lower in energy than
264 the two orientations that also contain four-fold coordinated borons.
265
266 A few differences come out when comparing our results with the ones by Bredow and
267 Islam.[22] They got surface energies of 0.34, 1.29, 1.12 and 2.21 J/m^2 for the same four
268 orientations, which they correlated with an increased number of dangling bonds per surface
269 area when increasing the energy. The stability of (100) and (011) surfaces is reversed.
270 Moreover, all surfaces but the most stable one show considerably larger surface energy
271 values compared to ours. Finally, all of our structures display no dangling bonds. These
272 issues are related to two key differences between our study and the literature one: we
273 exteneded our search for low energy surface structures to 1) structures featuring four-fold
274 coordinated B atoms, and 2) structures with alternative atomic terminations. This latter point
275 relates to symmetry analysis revealing that for all the four orientations there exists a repeating
276 unit along the non-periodic direction perpendicular to the slab that is made up of 3 B_2O_3
277 formula units. This implies that there are at least three different ways of terminating each
278 surface; this number gets even larger when considering that, for a given choice of terminating
279 B_2O_3 unit, there are several possible choices of atomic arrangements within the surface unit
280 cell. Exploitation of this property permitted us to identify the lowest energy structure for the
281 (100) surface.
282
283 **4. Conclusions**
284 In this study, we have adopted a quantum-mechanical approach exploiting a hybrid HF/DFT
285 Hamiltonian to investigate the structural, electronic and energetic properties of four low-
286 index surfaces of crystalline B_2O_3-I: (001), (011), (100) and (101).
287

This compound shows a great flexibility in terms of bond lengths and angles, thanks to the possibility of adopting both triangular BO_3 and tetrahedral BO_4 coordinations, and in addition to the further distortions allowed by both these structural units. We have demonstrated for the first time that the most stable surface terminations for the (011) and (001) orientations contain tetrahedral BO_4 units, featuring four-fold coordinated borons as well as three-fold coordinated oxygens. Energy for these two surfaces turns out to be higher than (101) and (100), that have only triangular BO_3 units.

A first implication of these findings is that all of the investigated low-index surfaces have no dangling bonds. This likely relates with the experimentally observed low surface reactivity of B_2O_3-I, except for the Lewis acid behaviour made possible by the empty p orbital in the three-fold coordinated B atoms. Surface terminations free from dangling bonds occur in other solids with mixed ionic-covalent bond character and flexible structural subunits, such as silica (SiO_2).[35] Notably, surfaces of these compounds can undergo hydroxylation to a variety of degrees at normal operational conditions;[52] therefore future computational investigations of the hydroxylation of B_2O_3-I surfaces represent a promising direction to further improve our understanding of their chemical and physical properties.

A second point of interest relates to the other forms in which B_2O_3 can be found in nature. Tetrahedral BO_4 units are the only building blocks of the high-pressure crystalline polymorph B_2O_3-II; besides, they are found in increasingly large fractions in the amorphous phase v-B_2O_3 when reaching higher pressures.[19] The occurrence of BO_4 units on some low-index surfaces of the low-pressure B_2O_3-I polymorph opens the way to investigating potentially relevant parallels in the structural and chemical properties of these forms. In particular, if on one hand the structurally complex amorphous phase is the one with the widest technological applications, the simple structure of B_2O_3-I makes it an excellent candidate as a structural

313 model for future computational studies on its surfaces properties as well as on surface
314 reconstruction.
315
316
317 **Acknowledgements**
318 This study has been supported by the National Computational Infrastructure (NCI), The
319 Australia and Pawsey Supercomputing Centre in Perth, as well as funds from the Australian
320 Research Council (ARC). N.A thanks Murdoch University for the award of a postgraduate
321 scholarship.
322
323 **Supporting Information.**
324 The Supporting Information is available free of charge on the ACS Publications website at
325 DOI: xxx. They present the relevant input/output files for structural optimisation and
326 analysis (distances, angles, charges) of the four surfaces and of the bulk.
327
328 **Notes**
329 The authors declare no competing financial interest.
330
331 **References**
332 1. Chawla, K. K. *Composite Materials: Science and Engineering*; Springer Science &
333 Business Media, 2012.
334 2. Chung, D. D. L. *Composite Materials: Science and Applications*; Springer Science &
335 Business Media, 2010.
336 3. dos Santos-Loff, D. M.; Kerner, R.; Micoulaut, M. Statistics of Boroxol Rings in
337 Vitreous Boron Oxide. *Europhys*. **1994**, *28*, 573-578.
338 4. Heitjans, P.; Indris, S. Diffusion and Ionic Conduction in Nanocrystalline Ceramics.
339 *J. Phys.: Condens. Matter*. **2003**, *15*, 1257-1289.

5. Indris, S.; Heitjans, P.; Roman, H. E.; Bunde, A. Nanocrystalline Versus Microcrystalline Li_2O:B_2O_3 Composites: Anomalous Ionic Conductivities and Percolation Theory. *Phys. Rev. Lett*. **2000,** *84*, 2889-2892.
6. Chawla, N.; Kerr, M.; Chawla, K. Monotonic and Cyclic Fatigue Behavior of High-Performance Ceramic Fibers. *J. Am. Ceram. Soc*. **2005**, *88*, 101-108.
7. Svanson, S.; Johansson, R. The Configuration of Three-Coordinated Boron in Vitreous and Crystalline Boron Oxide. *Acta chem. Scand.* **1969**, *23*, 635-646.
8. Warren, B.; Krutter, H.; Morningstar, O. Fourier Analysis of X-ray Patterns of Vitreous SiO_2 and B_2O_2. *J. Am. Ceram. Soc.* **1936**, *19*, 202-206.
9. Zachariasen, W. H. The Atomic Arrangement in Glass. *J. Am. Chem. Soc.* **1932**, *54*, 3841-3851.
10. Jellison, G. Jr.; Panek, L.; Bray, P.; Rouse Jr, G. Determinations of Structure and Bonding in Vitreous B_2O_3 by Means of B^{10}, B^{11}, and O^{17} NMR. *J. Chem. Phys*. **1977**, *66*, 802-812.
11. Johnson, P. A.; Wright, A. C.; Sinclair, R. N. A Neutron Diffraction Investigation of the Structure of Vitreous Boron Trioxide. *J. Non-Cryst. Solids.* **1982**, *50*, 281-311.
12. Mozzi, R. L.; Warren, B. The Structure of Vitreous Boron Oxide. *J. Appl. Clystallogr*. **1970**, *3*, 251-257.
13. Suzuya, K.; Yoneda, Y.; Kohara, S.; Umesaki, N. High Energy X-Ray Study of the Structure of Vitreous B_2O_3. *Phys. Chem. Glasses*. **2000**, *41*, 282-285.
14. Gurr, G.; Montgomery, P.; Knutson, C.; Gorres, B. The Crystal Structure of Trigonal Diboron Trioxide. *Acta Cryst.* **1970**, *26*, 906-915.
15. Prewitt, C.; Shannon, R. Crystal Structure of a High-Pressure Form of B_2O_3. *Acta Cryst.* **1968**, *24*, 869-874.
16. Nieto-Sanz, D.; Loubeyre, P.; Crichton, W.; Mezouar, M. X-Ray Study of the Synthesis of Boron Oxides at High Pressure: Phase Diagram and Equation of State. *Phys. Rev. B.* **2004,** *70*, 214108-214114.
17. Effenberger, H.; Lengauer, C. L.; Parthé, E. Trigonal B_2O_3 with Higher Space- Group Symmetry: Results of a Reevaluation. *Monatsh. Chem*. **2001**, *132*, 1515-1517.
18. Li, D.; Ching, W. Electronic Structures and Optical Properties of Low-and High-Pressure Phases of Crystalline B_2O_3. *Phys. Rev. B.* **1996**, *54*, 13616-13622.
19. Brazhkin, V.; Katayama, Y.; Trachenko, K.; Tsiok, O.; Lyapin, A.; Artacho, E.; Dove, M.; Ferlat, G.; Inamura, Y.; Saitoh, H. Nature of the Structural Transformations in B_2O_3 Glass Under High Pressure. *Phys. Rev. Lett.* **2008,** *101*, 035702-035706.

20. Zeidler, A.; Wezka, K.,; Whittaker, D. A.; Salmon, P. S.; Baroni, A.; Klotz, S.; Fischer, H. E., Wilding, M. C.; Bull C. L.; Tucker, M. G. Density-Driven Structural Transformations in B_2O_3 Glass. *Phys. Rev. B.* **2014,** *90*, 024206-024218.

21. Doyle, R. J. High-Molecular-Weight Boron Oxides in the Gas Phase. *J. Amer. Chem. Soc.* **1988,** *110*, 4120-4126.

22. Bredow, T., Islam, M. M. Theoretical Study of Low-Index Surfaces of Trigonal B_2O_3. *Surf. Sci.* **2008**, *602*, 2217-2221.

23. Dovesi, R.; Orlando, R.; Erba, A.; Zicovich-Wilson, C. M.; Civalleri, B.; Casassa, S.; Maschio, L.; Ferrabone, M.; De La Pierre, M.; D'Arco, P. CRYSTAL14: A Program for the ab Initio Investigation of Crystalline Solids. *Int. J. Quantum Chem.* **2014**, *114*, 1287-1317.

24. Dovesi, R.; Saunders, V. R.; Roetti, C.; Orlando, R.; Zicovich-Wilson, C. M.; Pascale, F.; Civalleri, B.; Doll, K.; Harrison, N. M.; Bush, I. J.; D'Arco, P.; Llunell, M.; Causà, M; Noël, Y. *CRYSTAL 2014 User's Manual*. 2014.

25. Bredow, T.; Gerson, A. R. Effect of Exchange and Correlation on Bulk Properties of MgO, NiO, and CoO. *Phys. Rev. B.* **2000**, *61*, 5194-5201.

26. Islam, M. M.; Bredow, T; Minot, C. Comparison of Trigonal B_2O_3 Structures with High and Low Space-Group Symmetry. *Chem. Phys. Lett.* **2006**, *418*, 565-568.

27. Perdew, J. P.; Vosko, J. A. S. H.; Jackson, K. A.; Pederson, M. R.; Singh, D. J.; Fiolhais, C. Atoms, Molecules, Solids, and Surfaces: Applications of the Generalized Gradient Approximation for Exchange and Correlation. *Phys. Rev. B.* **1992**, *46*, 6671-6687.

28. Perdew, J. P.; Ruzsinszky, A.; Csonka, G. I.; Vydrov, O. A.; Scuseria, G. E.; Constantin, L. A.; Zhou, X.; Burke, K. Restoring the Density-Gradient Expansion for Exchange in Solids and Surfaces. *Phys. Rev. Lett.* **2008,** *100*, 136406-136410.

29. Becke, A. D. Becke's Three Parameter Hybrid Method Using the LYP Correlation Functional. *J. Chem. Phys.* **1993**, *98*, 5648.

30. Lee, C.; Yang, W.; Parr, R. G. Development of the Colle-Salvetti Correlation- Energy Formula Into a Functional of the Electron Density. *Phys. Rev. B.* **1988,** *37*, 785-789.

31. Stephens, P.; Devlin, F.; Chabalowski, C.; Frisch, M. Ab Initio Calculation of Vibrational Absorption and Circular Dichroism Spectra Using Density Functional Force Fields. *J. Phys. Chem.* **1994**, *98*, 623-637.

32. Adamo, C.; Barone, V.; Toward Reliable Density Functional Methods Without Adjustable Parameters: The PBE0 Model. *J. Chem. Phys.* **1999,** *110*, 6158-6170.

33. De La Pierre, M.; Bruno, M.; Manfredotti, C.; Prencipe, F. M.; Manfredotti, C. The (100),(111) and (110) Surfaces of Diamond: An ab Initio B3LYP Study. *Mol. Phys.* **2014**, *112*, 1030-1039.
34. Civalleri, B.; Casassa, S.; Garrone, E.; Pisani, C.; Ugliengo, P. Quantum Mechanical ab Initio Characterization of a Simple Periodic Model of the Silica Surface. *J. Phys. Chem. B.* **1999**, *103*, 2165-2171.
35. Tosoni, S.; Civalleri, B.; Ugliengo, P. Hydrophobic Behavior of Dehydroxylated Silica Surfaces: A B3LYP Periodic Study. *J. Phys. Chem. C.* **2010**, *114*, 19984-19992.
36. Massaro, F. R.; Bruno, M.; Nestola, F. Configurational and Energy Study of the (100) and (110) Surfaces of the $MgAl_2O_4$ Spinel by Means of Quantum Mechanical and Empirical Techniques. *Cryst. Eng. Comm.* **2014,** *16*, 9224-9235.
37. Bruno, M.; Massaro, F.; Prencipe, M.; Demichelis, R.; De La Pierre, M.; Nestola, F. Ab Initio Calculations of the Main Crystal Surfaces of Forsterite (Mg_2SiO_4): A Preliminary Study to Understand the Nature of Geochemical Processes at the Olivine Interface. *J. Phys. Chem. C.* **2014**, *118*, 2498-2506.
38. Demichelis, R.; Bruno, M.; Massaro, F. R.; Prencipe, M.; De La Pierre, M.; Nestola, F. First-Principle Modelling of Forsterite Surface Properties: Accuracy of Methods and Basis Sets. *J. Comput. Chem.* **2015**, *36*, 1439-1445.
39. Heyd, J.; Peralta, J. E.; Scuseria, G. E.; Martin, R. L. Energy Band Gaps and Lattice Parameters Evaluated with the Heyd-Scuseria-Ernzerhof Screened Hybrid Functional. *J. Chem. Phys.* **2005**, *123*, 174101-174109.
40. Becke, A. D. Gradient Correction for the Nonlocal Part. *Phys. Rev. A.* **1988**, *38*, 3098-3100.
41. Monkhorst, H. J.; Pack, J. D. Special Points for Brillouin-Zone Integrations. *Phys. Rev. B.* **1976**, *13*, 5188-5192.
42. Civalleri, B.; D'Arco, P.; Orlando, R.; Saunders, V.; Dovesi, R. Hartree–Fock Geometry Optimisation of Periodic Systems with the CRYSTAL Code. *Chem. Phys. Lett.* **2001**, *348*, 131-138.
43. Doll, K. Implementation of Analytical Hartree–Fock Gradients for Periodic Systems. *Comput. Phys. Commun.* **2001**, *137*, 74-101.
44. Doll, K.; Saunders, V.; Harrison, N. Analytical Hartree–Fock Gradients for Periodic Systems. *Int. J. Quantum Chem.* **2001**, *82*, 1-31.

45. Pascale, F.; Zicovich-Wilson, C. M.; Lopez Gejo, F.; Civalleri, B.; Orlando, R.; Dovesi, R. The Calculation of the Vibrational Frequencies of Crystalline Compounds and Its Implementation in the CRYSTAL Code. *J. Comput. Chem.* **2004**, *25*, 888-897.
46. Dovesi, R.; Civalleri, B.; Roetti, C.; Saunders, V. R.; Orlando, R. *Reviews in Computational Chemistry*; John Wiley & Sons, Inc., 2005.
47. Dovesi, R.; De La Pierre, M.; Ferrari, A. M.; Pascale, F.; Maschio, L.; Zicovich-Wilson, C. M. The IR Vibrational Properties of Six Members of the Garnet family: A Quantum Mechanical ab Initio Study. *Am. Mineral*. **2011**, *96*, 1787-1798.
48. Demichelis, R.; Raiteri, P.; Gale, J. D.; Dovesi, R., Examining the Accuracy of Density Functional Theory for Predicting the Thermodynamics of Water Incorporation Into Minerals: The Hydrates of Calcium Carbonate. *J. Phys. Chem. C*. **2013**, *117*, 17814-17823.
49. Engberg, U. B_2O_3 Crystals Investigated by Plane-Wave Pseudopotential Calculations Using the Generalized-Gradient Approximation. *Phys. Rev. B*. **1997**, *55*, 2824-2830.
50. Huang, L.; Durandurdu, M.; Kieffer, J. New B_2O_3 Crystals Predicted from Concurrent Molecular Dynamics Simulations and First-Principles Calculations. *J. Phys. Chem. C.* **2007**, *111*, 13712-13720.
51. Brazhkin, V. V.; Katayama, Y.,; Inamura, Y.; Kondrin, M. V.; Lyapin, A. G. e.; Popova, S. V.; Voloshin, R. N. Structural Transformations in Liquid, Crystalline, and Glassy B_2O_3 Under High Pressure. *JETP Letters.* **2003**, *78*, 854-849.
52. Rimola, A.; Costa, D.; Sodupe, M.; Lambert, J.-F.; Ugliengo, P. Silica Surface Features and Their Role in the Adsorption of Biomolecules: Computational Modeling and Experiments. *Chem. Rev.* **2013**, *113*, 4216-4313.

Table 1. Structural and electronic properties of bulk B_2O_3–I.

	This work					Islam, Bredow and Minot[26]	Exp.[17]
	PBEsol	PW91	B3LYP	PBE0	**PW1PW**	PW1PW	
A	4.313	4.367	4.371	4.330	**4.334**	4.35	4.3358
C	8.095	8.501	8.718	8.366	**8.376**	8.39	8.3397
Δc (%)	-2.9	+1.9	+4.5	+0.3	**+0.4**	+0.6	--
d(B-O_a)	1.378	1.380	1.373	1.370	**1.371**	1.376	1.376
d(B-O_a')	1.375	1.375	1.367	1.365	**1.366**	1.374	1.374
d(B-O_b)	1.368	1.369	1.362	1.360	**1.361**	1.370	1.357
θ(O_a-B-O_a')	120.1	120.5	120.6	120.5	**120.4**	--	120.5
θ(O_a-B-O_b)	116.3	116.3	116.6	116.4	**116.5**	--	116.4
θ(O_a'-B-O_b)	123.0	122.9	122.6	122.8	**122.8**	--	123.2
q(B)	+0.934	+0.935	+1.015	+1.048	**+1.029**	--	--
q(O_a)	-0.616	-0.614	-0.665	-0.688	**-0.676**	--	--
q(O_b)	-0.637	-0.642	-0.700	-0.718	**-0.705**	--	--
E_{gap}	6.44	6.41	8.57	9.21	**8.66**	9.1	--

Lengths are in Å, angles in °, net Mulliken charges in |e| units, E_{gap} in eV. *Δc* is the percent deviation of the *c* cell parameter with respect to the experimental value. Data obtained with the PW1PW Hamiltonian in the present work are in bold for ease of reading.

Table 2. Surface energies γ (J/m^2) of the low-index surfaces of B_2O_3-I.

	This work					Bredow and Islam[22]
	PBEsol	PW91	B3LYP	PBE0	**PW1PW**	PW1PW
(001)	0.780	0.816	0.875	0.884	**0.882**	2.21
(011)	0.675	0.691	0.824	0.743	**0.735**	1.12
(100)	0.576	0.311	0.240	0.400	**0.396**	1.29
(101)	0.329	0.210	0.188	0.254	**0.254**	0.34

Data obtained with the PW1PW Hamiltonian in the present work are in bold for ease of reading.

476 Table 3. Bond lengths (d, Å) and angles (θ, ˚) for surface B atoms of the low-index surfaces
477 of B_2O_3-I**.**

		d			θ		
(001)		O1	O2	O3*	O1,O2	O1,O3*	O2,O3*
	B1	1.335	1.334	1.455	117.2	119.0	123.5
		O1	O2	O3*	O1,O2	O1,O3*	O1,O4
	B2*	1.383	1.378	1.847	114.1	101.3	113.7
		O4	--	--	O2,O3*	O2,O4	O3*,O4
	“	1.431	--	--	109.9	113.6	102.7
(011)		O1	O2	O3	O1,O2	O1,O3	O2,O3
	B1	1.384	1.374	1.386	120.2	120.6	119.2
		O2	O4	O5	O2,O4	O2,O5	O4,O5
	B2	1.371	1.411	1.348	121.8	121.5	116.8
		O4	O6	O7*	O4,O6	O4,O7*	O6,O7*
	B3	1.355	1.328	1.526	119.9	126.6	113.6
		O6	O7*	O8	O6,O7*	O6,O8	O6,O9
	B4*	1.400	1.642	1.467	104.8	108.0	116.3
		O9	--	--	O7*,O8	O7*,O9	O8,O9
	“	1.428	--	--	115.4	103.1	109.5
		O1	O7*	O8	O1,O7*	O1,O8	O7*,O8
	B5	1.344	1.469	1.347	119.8	122.0	118.2
(100)		O1	O2	O3	O1,O2	O1,O3	O2,O3
	B1	1.348	1.362	1.365	121.2	122.6	116.2
		O1	O2	O4	O1,O2	O1,O4	O2,O4
	B2	1.364	1.358	1.347	120.1	119.7	120.0
		O4	O5	O6	O4,O5	O4,O6	O5,O6
	B3	1.344	1.356	1.368	118.0	124.5	117.5
		O5	O7	O8	O5,O7	O5,O8	O7,O8
	B4	1.360	1.362	1.371	118.5	120.0	121.3
		O3	O7	O9	O3,O7	O3,O9	O7,O9
	B5	1.354	1.358	1.371	121.5	118.5	119.9
(101)		O1	O2	O3	O1,O2	O1,O3	O2,O3
	B1	1.367	1.357	1.381	121.1	119.0	118.1
		O1	O4	O5	O1,O4	O1,O5	O4,O5
	B2	1.376	1.353	1.379	120.3	118.5	120.1
		O4	O6	O7	O4,O6	O4,O7	O6,O7
	B3	1.368	1.346	1.378	117.8	117.8	124.1
		O6	O8	O9	O6,O8	O6,O9	O8,O9
	B4	1.339	1.371	1.377	117.0	123.1	119.7
		O2	O8	O9	O2,O8	O2,O9	O8,O9
	B5	1.354	1.356	1.375	122.5	116.5	121.0

478 Atomic labels as in Figures 3 to 6. Asterisks are used to mark either four-fold coordinated B
479 atoms or three-fold coordinated O atoms.

480

481 Table 4. Net Mulliken charges (|e|) for the surface B atoms, and corresponding chemically

482 bound O atoms, of the low-index surfaces of B_2O_3-I.

	B1	B2	B3	B4	B5				
(001)	+0.893	+0.986*	--	--	--				
(011)	+1.019	+0.955	+0.927	+0.992*	+0.910				
(100)	+0.896	+0.852	+0.820	+0.830	+1.003				
(101)	+0.978	+0.802	+0.959	+0.908	+0.917				
	O1	O2	O3	O4	O5	O6	O7	O8	O9
(001)	-0.552	-0.548	-0.804*	-0.710	--	--	--	--	--
(011)	-0.593	-0.634	-0.643	-0.579	-0.580	-0.548	-0.797*	-0.625	-0.610
(100)	-0.551	-0.617	-0.675	-0.531	-0.522	-0.637	-0.578	-0.630	-0.674
(101)	-0.558	-0.666	-0.687	-0.539	-0.619	-0.579	-0.668	-0.588	-0.649

483 Notation as in Table 3.

484

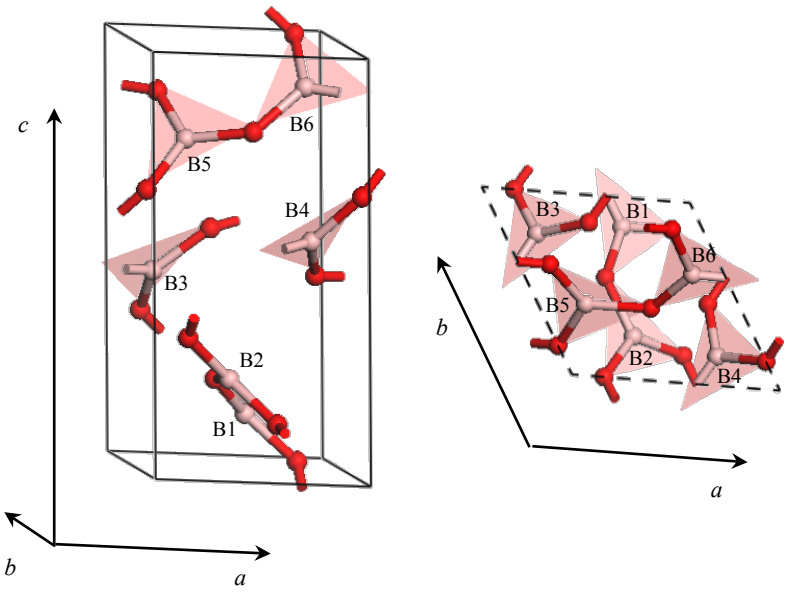

Figure 1. The primitive unit cell of bulk B_2O_3-I (side and top views). Light pink and red spheres refer to boron and oxygen atoms, respectively.

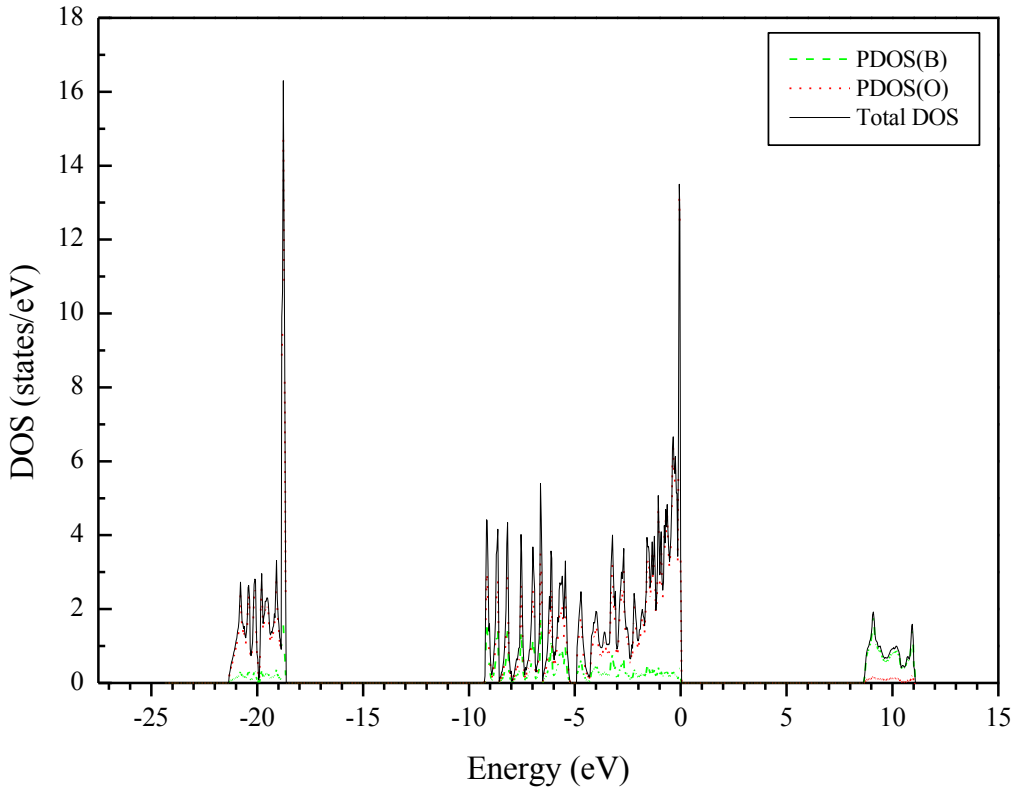

Figure 2. Total (DOS) and partial (PDOS) electronic densities of states for bulk B_2O_3-I.

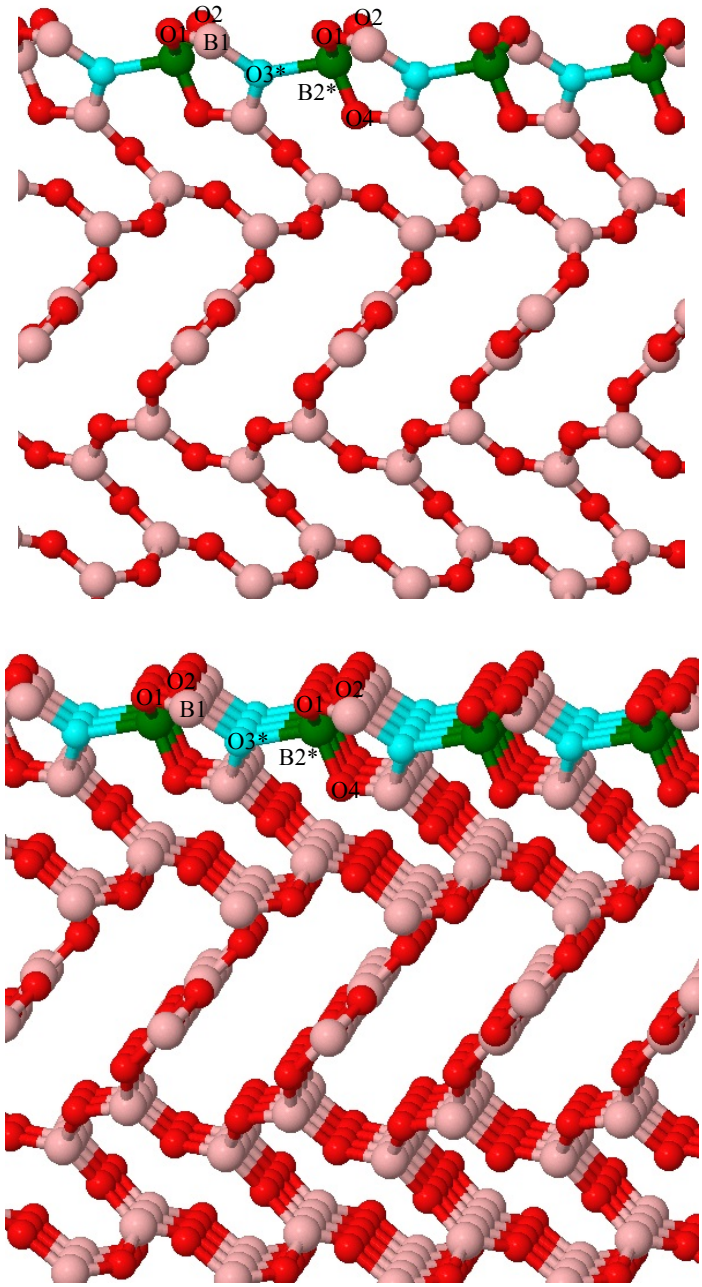

Figure 3. Atomic structure of the B_2O_3-I (001) surface. Both side and tilted views are shown. Labels are used to name rows (orthogonal to the plane of the document) of symmetry irreducible surface B atoms, as well as rows of the O atoms that are bound to the former. Asterisks are used to mark either four-fold coordinated B (green spheres) atoms or three-fold coordinated O atoms (cyan spheres).

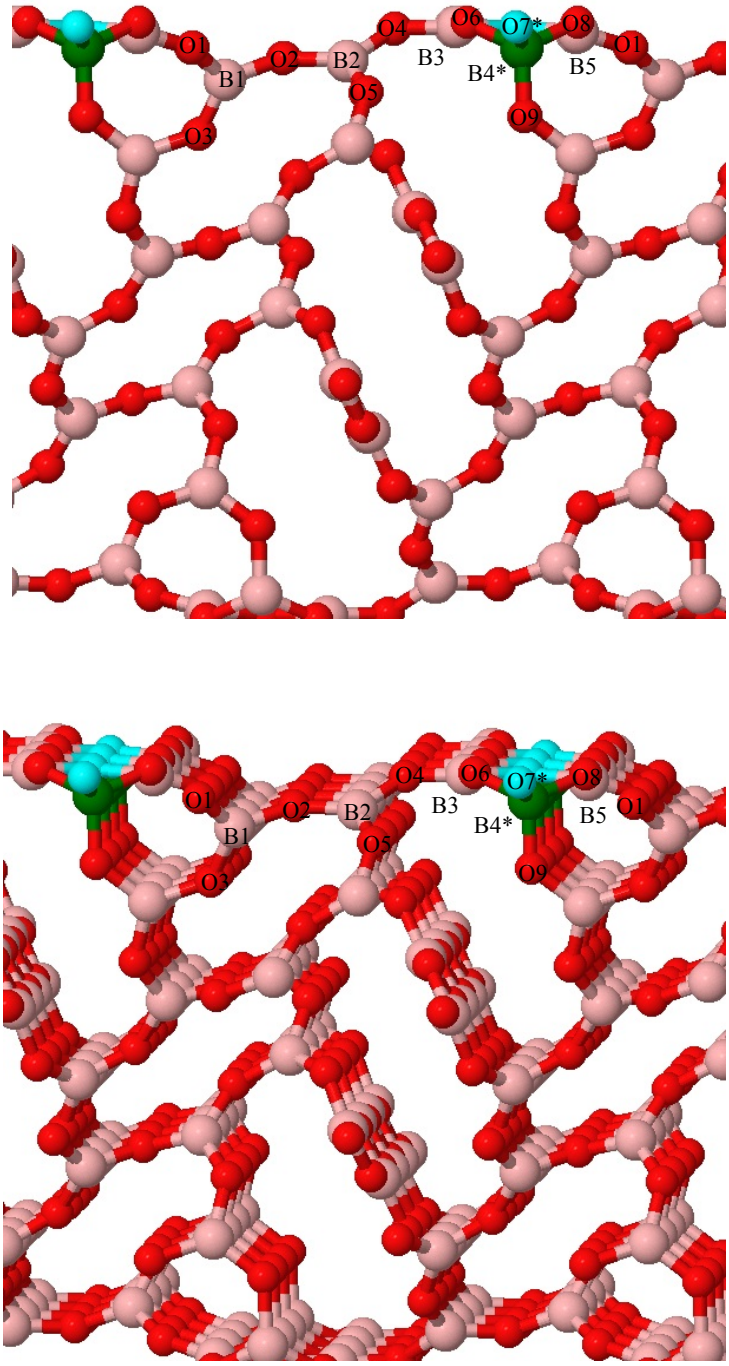

Figure 4. Atomic structure of the B_2O_3-I (011) surface. Refer to the caption to Figure 3 for more details.

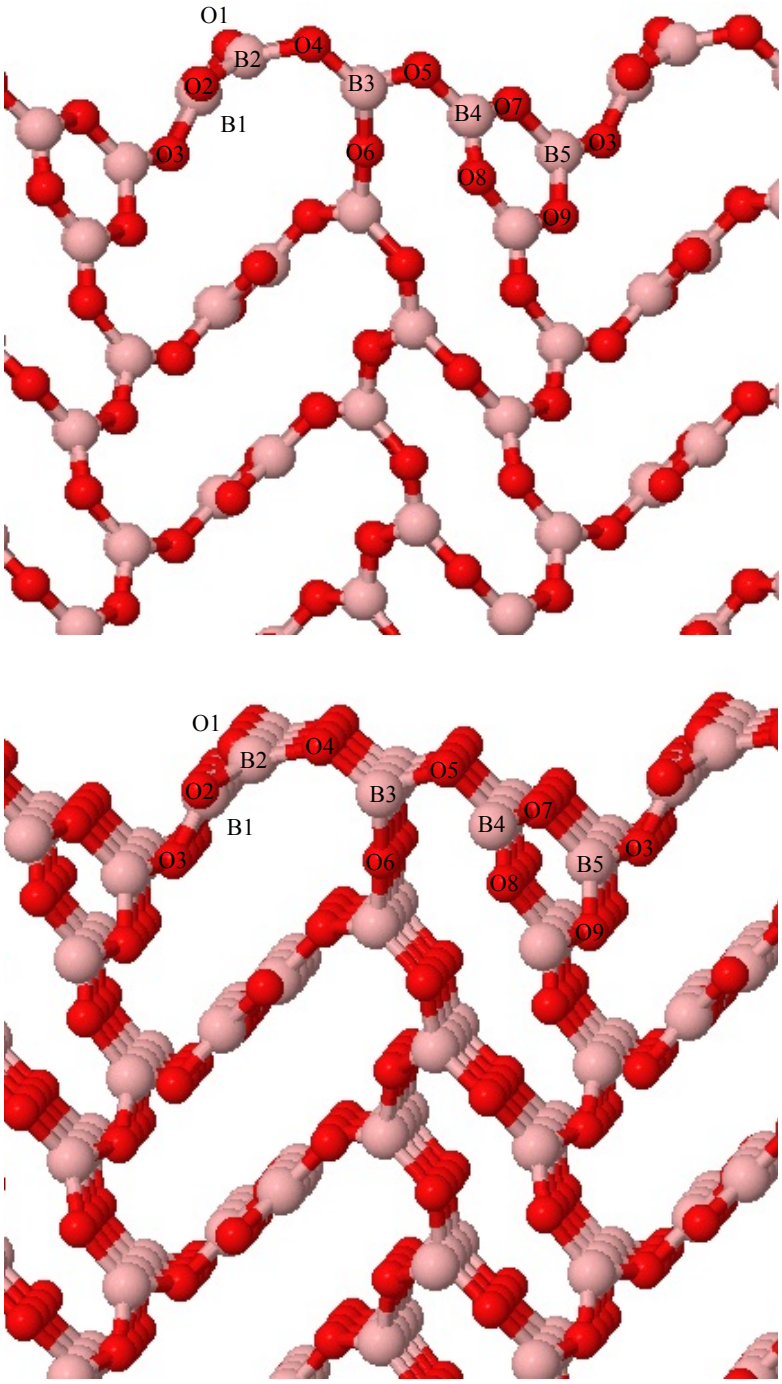

Figure 5. Atomic structure of the B_2O_3-I (100) surface. Refer to the caption to Figure 3 for more details.

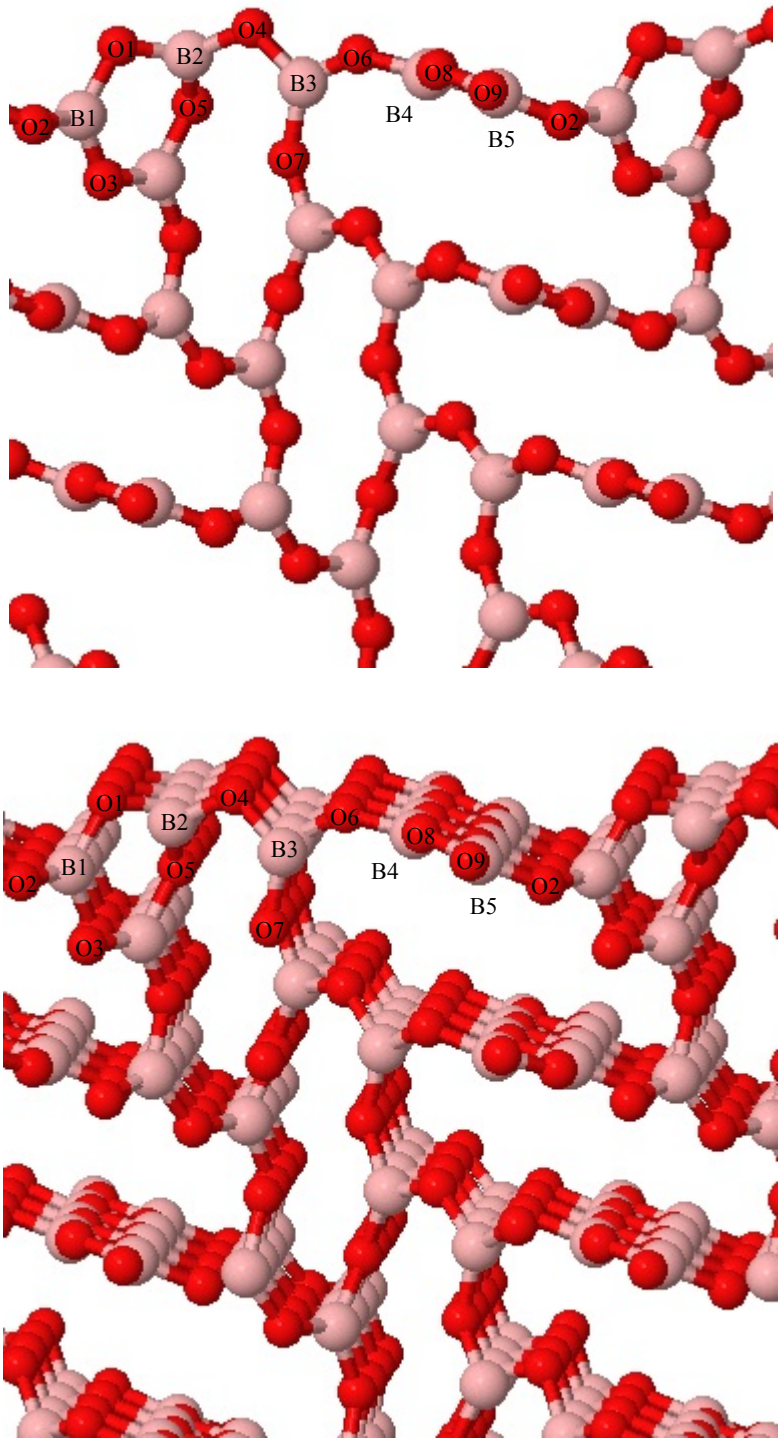

Figure 6. Atomic structure of the B_2O_3-I (101) surface. Refer to the caption to Figure 3 for more details.

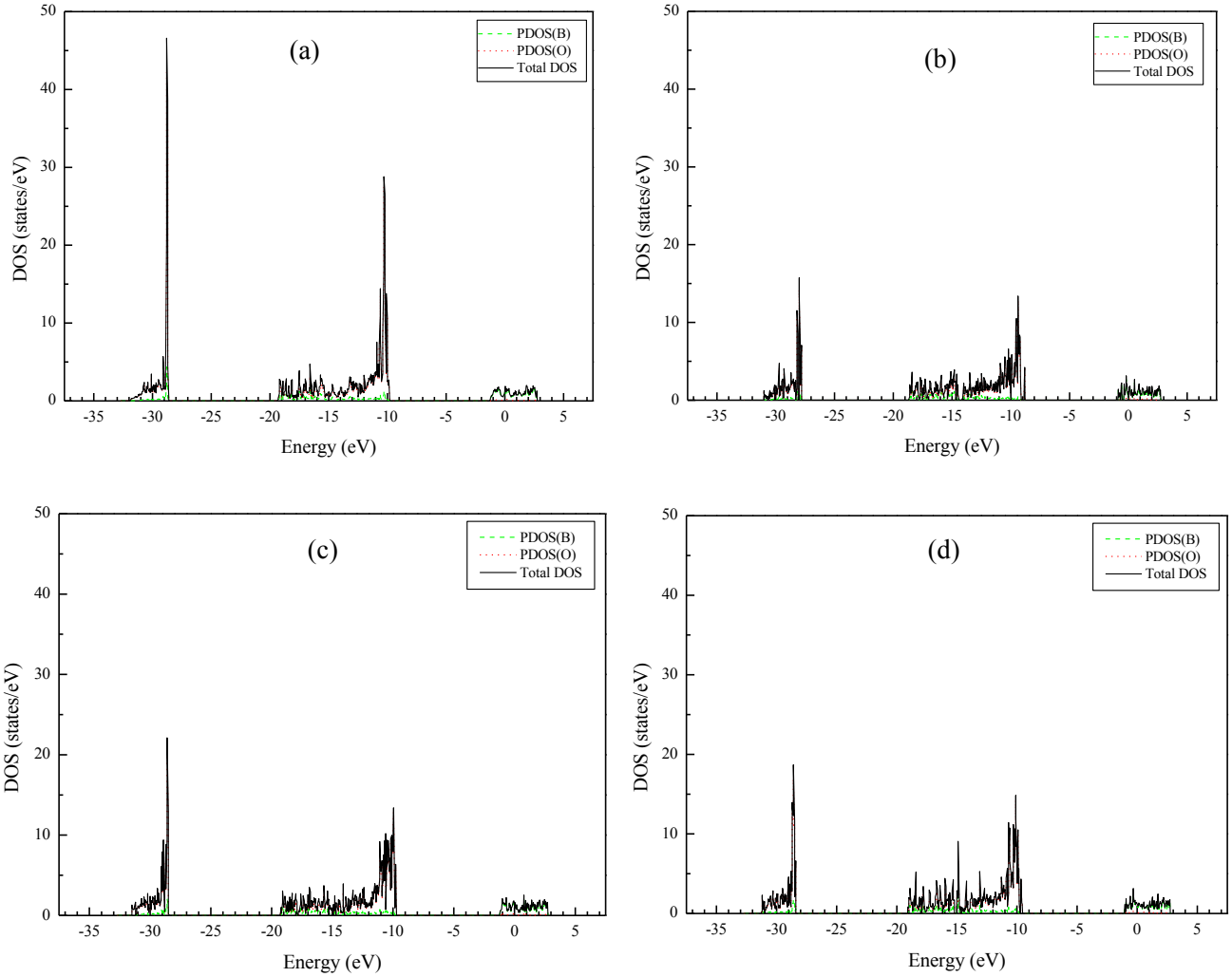

Figure 7. Total density of states (DOS) and projected density of states (PDOS) for the (a) (001), (b) (011), (c) (100), and (d) (101) surfaces of B_2O_3-I.